Published in "The Journal of Physical Chemistry B 118(16): 4261–4272, 2014"
which should be cited to refer to this work.

Fragment Orbital Based Description of Charge Transfer in Peptides Including Backbone Orbitals

Alexander Heck,[†] P. Benjamin Woiczikowski,[†] Tomáš Kubař,[†] Kai Welke,[†] Thomas Niehaus,[‡] Bernd Giese,[¶] Spiros Skourtis,[§] Marcus Elstner,[†] and Thomas B. Steinbrecher*,[†]

[†]Department for Theoretical Chemical Biology, Institute for Physical Chemistry, Kaiserstrasse 12, Karlsruhe Institute of Technology, 76131 Karlsruhe, Germany

[‡]Department of Physics, University of Regensburg, 93053 Regensburg, Germany

[¶]Department of Chemistry, University of Fribourg, Chemin du Musee 9, CH-1700 Fribourg, Switzerland

[§]Department of Physics, University of Cyprus, PO Box 20537, Nicosia 1678, Cyprus

ABSTRACT: Charge transfer in peptides and proteins can occur on different pathways, depending on the energetic landscape as well as the coupling between the involved orbitals. Since details of the mechanism and pathways are difficult to access experimentally, different modeling strategies have been successfully applied to study these processes in the past. These can be based on a simple empirical pathway model, efficient tight binding type atomic orbital Hamiltonians or *ab initio* and density functional calculations. An interesting strategy, which allows an efficient calculations of charge transfer parameters, is based on a fragmentation of the system into functional units. While this works well for systems like DNA, where the charge transfer pathway is naturally divided into distinct molecular fragments, this is less obvious for charge transfer along peptide and protein backbones. In this work, we develop and access a strategy for an effective fragmentation approach, which allows one to compute electronic couplings for large systems along nanosecond time scale molecular dynamics trajectories. The new methodology is applied to a solvated peptide, for which charge transfer properties have been studied recently using an empirical pathway model. As could be expected, dynamical effects turn out to be important, which emphasizes the importance of using effective quantum approaches which allow for sufficient sampling. However, the computed rates are orders of magnitude smaller than experimentally determined, which indicates the shortcomings of present modeling approaches.

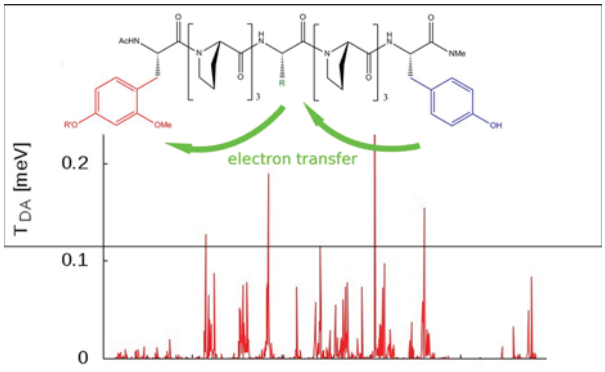

INTRODUCTION

Charge transfer (CT) in biomolecules is a fundamental process that has been subject of intense scientific study for more than 50 years.[1−4] It is highly relevant in the understanding of functional as well as pathological cellular processes, ranging from respiration and photosynthesis to DNA damage and repair.[5−7] Our theoretical understanding of molecular CT has increased tremendously since the pioneering studies by Marcus and others,[8−16] but a complete detailed description on the molecular level remains elusive.

Several approaches exist to compute the electronic couplings, ranging from empirical pathway models,[17−19] over tight-binding based[20,21] to *ab initio* or density functional calculations.[22−25] Most of these quantum approaches are based on an atomic orbital description to compute charge transfer parameters, which becomes very costly for large systems, even when using extended Hückel or tight-binding Hamiltonians, because the computer time scales cubic with the number of atomic orbitals involved. An additional computational challange is the need for sampling along MD trajectories. The biochemical transfer of electrons over many nanometers through large protein assemblies involves dynamical changes that occur on time scales ranging from subpicosecond changes in electronic structure to microsecond or even slower conformational changes. Especially the interplay between the atomic structural fluctuations and the electron dynamics has become a focus for CT studies in biochemical systems.[26−31] The increased sophistication and accuracy of experimental techniques, often providing information obtained at the single molecule level,[32−34] provides challenges for improving CT models on the simulation side.

One way to improve computational performance is to use a fragment orbital (FO) description, because this leads to a linear scaling of computer time with system size. This idea has been explored in early work on tunneling through organic molecules[35−37] showing, that an efficient method for large

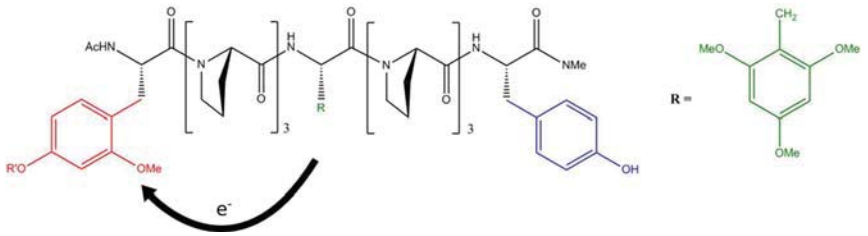

Figure 1. Model peptide synthesized for the study of CT. The N-terminal non-natural aromatic amino acid residue contains a photoexcitable group in the 4-position, which fragments and forms a radical cation upon UV exposure. The synthesis and reaction mechanism of the site-specific charge injection system is described in detail in refs 44−48. CT occurs in a two-step hopping process involving N-terminal, central and C-terminal amino acid side chains. In this work, CT calculations are focused on the initial hopping step, shown in the figure.

systems can be based on the calculation of matrix elements for smaller molecules, as long as the chemical environment is comparable. Kurnikov and Beratan[38] have further elaborated the idea of fragment Hamiltonians, where a large molecule is partitioned into overlapping fragments, from which the Hamiltonian can be built in a computational efficient way.

In the last years, we have developed a FO approach, which uses the semiempirical DFTB Hamiltonian[39] to compute the charge transfer parameters. This approach is very efficient on the one hand, allowing to sample along MD trajectories in the nanosecond regime, and computationally robust, since it uses the FO approach.[39,40] We have applied this method to systems, where the electron transfer pathway is naturally divided into molecular fragments, like in DNA, organic materials or the tryptophane triad in photolyase. The fragment Hamiltonian has been either used to compute transmission or currents in the framework of Landauer theory,[41] or to solve the time-dependent Schrödinger equation, which allows to propagate the electronic degrees of freedom.[42,43] In this work, one major aim is to investigate the possibility of fragmentation of extended molecules like polypeptides. For this purpose, covalent bonds have to be intersected in order to construct a fragment Hamiltonian for the entire system. As in previous work,[38] this leads to significant computational savings. In contrast, we divide into nonoverlapping fragments, which allows to use the method in propagation schemes[42,43] and in tunneling calculations. The coupling to the chemical environment is included via a QM/MM formalism, which turns out to be important in particular in polar environments. The fluctuations of the solvent and protein environment have a huge impact on the active sites, which govern the charge transfer.[39,40] This leads to fluctuations of the charge transfer energetics, which can be a crucial factor to understand the mechanism and dynamics of CT. As Kurnikov and Beratan[38] have pointed out, the use of different methods can lead to very different results. A particular challenge is the application of DFT methods in this context. The problem of self-interaction (SI) within DFT, as long as no specifically corrected DFT functional is used, leads to an incorrect description of the HOMO (LUMO) levels of the fragments. Since these levels along the charge transfer pathway determine the energetics and thereby the charge transfer rate, an incorrect description can easily lead to errors of several orders of magnitude. The FO-Hamiltonian, besides being computationally efficient, allows to correct the site energies on the basis of high level reference calculations, which is a major advantage over a direct atomic orbital based calculation of bridge-mediated donor−acceptor couplings.

As an application system, we chose CT in a small peptide, which we have studied previously, since the charge transfer pathway seems to be well-defined.[44] In that work, however, we only could study the direct CT between donor and acceptor neglecting the bridge within the FO approach, other pathways have been investigated using an empirical pathway model. Now, we also include the peptide backbone into the FO description.

The peptide model system was developed in the group of B. Giese (Figure 1). The positive charge on the N-terminal amino acid is generated by laser flash photolysis, followed by two charge transfer reactions.[49−52] In a first step the hole is transferred to the central amino acid side chain until in a subsequent event it is transferred to the final hole acceptor at the C-terminal end. Since CT can be photoinduced selectively and the involved intermediates are observable by their transient absorption spectrum, this peptide system offers an excellent opportunity to study biochemical CT under defined conditions. In the following we are focusing on the first CT reaction between the central bridging amino acid residue trimethoxy phenylalanine (TMP) and the remainder of the N-terminal photoexcitable group, modeled as dimethoxy substituted phenylalanine (DMP). Direct, through space pathways will be considered as well as backbone mediated transfer.

METHODOLOGY

In order to obtain a coarse grained model Hamiltonian for the description of CT, the system is divided into fragments (Figure 2), namely into donor and acceptor as well as several peptide

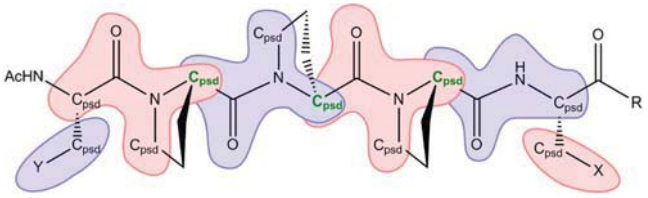

Figure 2. Schematic fragmentation of the system into electron donor (X), acceptor (Y), and four peptide bonds. Backbone fragments show overlapping capping atoms (green).

fragments, depending on the length of the peptide backbone bridging them. This allows one to compute a Hamiltonian

$$H = \begin{pmatrix} \varepsilon_A & V_{A1} & \cdots & V_{AD} \\ V_{1A} & \varepsilon_1 & \cdots & V_{1D} \\ \vdots & \vdots & \ddots & \vdots \\ V_{DA} & V_{D1} & \cdots & \varepsilon_D, \end{pmatrix} \quad (1)$$

where the diagonal elements ε represent the energy of the fragments with the charge localized at donor (D), acceptor (A),

and the bridge fragments (1, 2, 3, ...) respectively, and off-diagonal elements describe the coupling between these states. For the calculation of these matrix elements a fragment orbital approach is used, where the charge localized states are described by the HOMOs of the fragments:

$$H_{ij} = \langle \phi_i | \hat{H} | \phi_j \rangle = \sum_{\mu\nu} c_\mu^i c_\nu^j \langle \eta_\mu | \hat{H} | \eta_\nu \rangle = \sum_{\mu\nu} c_\mu^i c_\nu^j H_{\mu\nu} \tag{2}$$

where ϕ_i are fragment orbitals consisting of atomic orbitals η_μ. Since the fragment orbital approach is a very robust method to calculate the matrix elements, it can readily be applied to an ensemble of structures during a MD simulation to obtain a time dependent Hamilton matrix, which is a desirable feature regarding the flexibility of proteins and peptides in particular.

If the bridge is energetically well separated from donor and acceptor, an effective electronic coupling between donor and acceptor can be computed via partitioning H into a donor–acceptor subspace P and a bridge subspace Q. Formulating the effective Schrödinger equation for P, as discussed previously,[38,53−55] gives both the direct and bridge-mediated coupling. In this formalism, the total electronic coupling (off-diagonal element of the donor–acceptor subspace Hamiltonian) is calculated as

$$\begin{aligned} \langle \phi_D | \hat{H}_{PP}^{\text{eff}} | \phi_A \rangle &= V_{DA} + T_{DA} \\ &= \langle \phi_D | \hat{H}_{PP} | \phi_A \rangle + \sum_{ij} \langle \phi_D | \hat{H}_{PQ} | \phi_i^{\text{bridge}} \rangle \\ &\quad \times \langle \phi_i^{\text{bridge}} | (E_m I_{QQ} \hat{H}_{QQ})^{-1} | \phi_j^{\text{bridge}} \rangle \\ &\quad \times \langle \phi_j^{\text{bridge}} | \hat{H}_{QP} | \phi_A \rangle \end{aligned} \tag{3}$$

where i and j run over all bridge levels and E_m is the averaged orbital energy level of donor and acceptor. Equation 3 involves both the direct donor–acceptor coupling V_{DA} and the bridge-mediated components of the overall coupling, T_{DA}. Here, the P subspace contains the HOMOs of donor and acceptor, while the Q subspace contains all relevant peptide backbone fragment orbitals (see below for orbital selection).

Furthermore, the fragment orbital Hamiltonian can also be used in a more sophisticated direct propagation of the charge using the time-dependent Schrödinger equation. This approach is necessary if bridge levels are not well separated from donor and acceptor and therefore might be populated by the hole. To capture the response of the environment to the moving charge nonadiabatic molecular dynamics can be performed as we have done before in the case of CT in DNA.[42,43]

COMPUTATIONAL DETAILS

System Setup and Molecular Dynamics Simulations. For the MD simulation the peptide was built and parametrized as described previously,[44] using the Amber99SB all-atom force field.[56] The alkoxy-substituted donor, acceptor and relay side chains were built by adapting existing GAFF parameters for bonded terms and fitting partial charges according to the RESP procedure.[57] The experimentally used water-acetonitrile solvent mixture was represented by TIP4P water molecules[58,59] combined with a united-atom acetonitrile model[60] that reproduced the experimentally known density and molecular dipole of acetonitrile reasonably well in test calculations.

All MD simulations were conducted using version 4.5 of the *Gromacs* MD package.[61,62] For equilibration, temperature and pressure were controlled by a Berendsen coupling algorithm, with separate temperature coupling groups for solute, water and acetonitrile solvent. The smooth particle-mesh Ewald model with a 10 Å direct space cutoff was used to describe long-range electrostatics, and the same cutoff was used for van der Waals interactions. A time step of 2 fs was used while constraining bonds involving hydrogen atoms using the LINCS algorithm.[63] All of the data collection MD simulations were preceded by a standard equilibration protocol involving 100 steps of energy minimization, a 20 ps temperature equilibration to 300 K in the *NVT* ensemble and a final 400 ps *NPT* density equilibration. For production simulations, the Nosé–Hoover thermostat and the Parrinello–Rahman barostat were used.

QM Calculations. For the QM calculations the efficient approximate DFT method DFTB2[64,65] is used since several thousand SCF calculations have to be performed for structures taken along classical MD trajectories. Furthermore, we aim to apply this method also to CT in proteins where significant larger QM regions might be necessary. To model the dynamics of the system and the influence of the environment, a QM/MM model is applied. The computations involve several steps:

Conformational snapshots of the complete solvated peptide system are obtained from classical MD simulations as describe above. The QM fragments for donor, acceptor and bridge groups are identified and saturated by means of pseudoatoms (see below for details of the capping approach). A separate DFTB2 calculation is conducted for each fragment, while including the electric effects of solvent and of the remainder of the peptide in the form of their MM atomic point charges. Since a nonpolarizable force field is used, the fluctuations of the electrostatic potential would be overestimated. To correct this shortcoming, the magnitude of the external field is scaled down by a factor of 1/1.5 for the QM calculations as suggested previously.[42,43] The CT Hamiltonian for the entire donor–bridge–acceptor system is then constructed in the FO formalism[66,67] from a basis set constituting the relevant MOs ϕ_m^{HO} of the individual fragments m (see below for details on MO selection), taking the electric field induced by the surrounding medium into account via point charges as above. The basis is then orthogonalized via Löwdin's method.[68]

In QM/MM calculations, special care has to be taken to conserve the charge of the whole system, since in general a partially charged part of the system is replaced by a QM region with integer charge. Two common approaches that are used for electrostatic embedding of the QM zone are either to shift MM pointcharges that are too close to the capping atom to MM atoms further apart or to delete charges in the boundary region. In the latter approach typically an entire charge group of the force field is deleted. The amber force field applied for MD in this work uses whole amino acids as charge groups. The deletion of such a charge group will be problematic in the case of charged amino acids, since this would change the electrostatic potential tremendously. A solution would be to use force fields with smaller charge groups like, e.g., the CHARMM force field. Since amber force field parameters for the nonstandard amino acids of the model system were already at hand, we decided to use the amber force field for the MD but modify the pointcharges slightly for the QM calculations to obtain significant smaller charge groups similar to the CHARMM force field. For this purpose, each of the peptide residues is divided into three charge groups, comprising (a) the carbonyl moiety, (b) the side chain, and (c) the amide nitrogen together with C_α–H_α. Furthermore, partial charges were

ignored for computing environmental effects if any atom of their charge group overlapped with a fragment. Amino acid atom partial charges had to be modified only slightly to generate integer charges for the groups.

Fragmentation of the Peptide Backbone. For the FO approach used here, an appropriate fragmentation of the system into QM fragments needs to be conducted. The fragmentation of donor and acceptor is straightforward since these are usually either cofactors or aromatic side chains, where the $C_\alpha - C_\beta$ bonds can be cut to obtain independent moieties. For the case of CT involving a protein backbone, a proper fragmentation procedure is less clear. Since the experiments by Giese et al. (see above) use a polyproline linker between donor and acceptor special care was taken of peptide bonds involving proline. A fragmentation of the conjugated peptide bond should be avoided, therfore the question is which of its substituents should be included in the QM system. We have computed vertical IP values using DFTB2 and the ΔSCF approach in which the IP is given by

$$\mathrm{IP} = E^{SCF}_{\mathrm{cation}} - E^{SCF}_{\mathrm{neutral}} \quad (4)$$

using the relaxed structure of the neutral fragment for both SCF calculations. The IP values for the possible fragments 1-acetylpyrrolidine, *N,N*-dimethylacetamide, *N*-methylacetamide, acetamide, *N,N*-dimethylformamide and formamide are given in Table 1 and show that the IP of *N,N*-dimethylacetamide

Table 1. IP Values for Peptide Backbone QM Fragments Considered Here[a]

fragment	IP(ΔSCF) [eV]
1-acetylpyrrolidine	8.73
N,N-dimethylacetamide	8.93
N-methylacetamide	9.39
acetamide	9.74
N,N-dimethylformamide	9.20
formamide	10.13

[a]The result for *N,N*-dimethylacetamide closely reproduces the IP of the largest backbone model 1-acetylpyrrolidine.

(NNDMA) matches closely that of the largest fragment, 1-acetylpyrrolidine. Since NNDMA is significantly smaller than 1-acetylpyrrolidine, it was chosen for the backbone fragmentation to reduce the computational effort in the following. For all of the remaining amino acid residues except proline, the largest possible fragment *N*-methylacetamide was chosen instead.

Description of Backbone Orbitals. The selection of the orbitals that represent the electron hole state is a nontrivial task for peptide bond fragments. It is known from photoelectron spectroscopy that the orbitals n_0 (oxygen lone pair) and π_1 (nonbinding π) represent the two MOs of highest energy in amides (Figure 3). For NNDMA, the π_1-orbital energy is known experimentally to be 0.3 eV above that of n_0 in vacuum.[69]

We have computed the HOMO and HOMO-1 energies of NNDMA using several common quantum chemistry approaches with the TZVP basis set afte optimizing the structure using B3LYP. The results (Table 2) show large variations in absolute energies as well as in the ordering of the MOs. The expected ordering and energetic separation of the two orbitals is not reproduced by any calculation, and the nonhybrid density functional approaches PBE and DFTB even switch the orbital order. Interestingly, comparing the N and $N-1$ electron

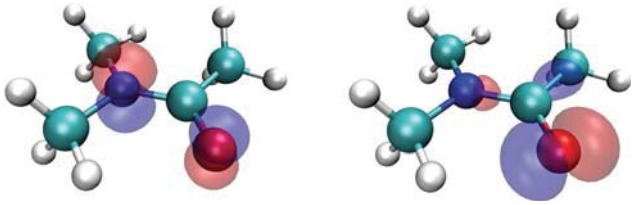

Figure 3. Two highest occupied MOs in the amide NNDMA, the orbitals π_1 (left) and n_0 (right). Orbitals were visualized in VMD.[70]

Table 2. Orbital Energies for *N,N*-Dimethylacetamide Computed Using Various Levels of QM Theory with the TZVP Basis Set[a]

QM level	E(HOMO) [eV]	E(HOMO-1) [eV]
HF	−10.05 (π_1)	−11.33 (n_0)
B3LYP	−6.70 (π_1)	−6.89 (n_0)
PBE	−5.51 (n_0)	−5.62 (π_1)
DFTB	−5.46 (n_0)	−5.75 (π_1)
DFTB-GW	−6.61 (n_0)	−7.90 (π_1)
DFT-GW	−8.20 (π_1)	−8.52 (n_0)

[a]The type of MO is indicated in brackets. The experimentally known energetic separation of the π_1 orbital 0.3 eV above n_0 is not reproduced by any approach except DFT-GW. PBE and DFTB switch the orbital order.

system for HF shows the distribution of the total electron density difference to correspond to the n_0-orbital, as found for the case of formamide previously[71] even though the π_1 orbital lies 1.3 eV higher in the neutral molecule. Clearly, a higher level of quantum theory calculation is needed to represent the MO structure of NNDMA in vacuum accurately.

Additional calculation were performed at the MP2/def2-TZVP level. When using the MP2 perturbation theory[72,73] to describe NNDMA, no discrete orbital energies can be computed any longer. When natural orbitals are constructed from the results,[74] HOMO and LUMO take the shape of π_1 and π_2 orbitals, so the MP2 correction yields the expected orbital order. However, no pure n_0 orbital was found for HOMO-1 and HOMO-2, which are σ orbitals instead.

As a further method, the multireference method CASSCF-(8,5)/def2-TZVPP[75] as implemented in the *Orca* QM package[76] was used to determine the frontier orbitals. An occupation number of 1.96 was found for the π_1 orbital, significantly smaller than the value found for the n_0 orbital. This suggests that π_1 should be considered the HOMO of NNDMA.

Finally, we turn to the GW method[77−79] in order to improve the results of our DFT calculations. For DFTB, the GW correction still yields the n_0 orbital as HOMO. DFT-GW calculations[88] correctly describe the experimentally known orbital order of the orbitals, with π_1 0.32 eV above n_0.

Summarily, only high-level QM calculations reproduce the experimental ordering of the π_1 orbital of NNDMA to be 0.3 eV above the n_0 energy in vacuum, but neither DFTB nor common *ab initio* approaches are able to correctly identify the orbital order. The wrong relative MO energies in DFTB, however, can be easily corrected by adding a constant shift of 0.61 eV for the n_0 orbital to reproduce the relative DFT-GW values.

Pseudoatom Fragment Capping. For the individual QM calculations the fragment boundaries must be treated in a way to obtain saturated molecules. Typical approaches use capping groups, either link atoms, placed at a selected distance along the

bond axis crossing the QM boundary region, or connection atoms, which occupy the same position as the atom outside of the fragment (e.g., the C_α and C_γ atoms in the case of a proline peptide bond fragment).[80−83] In the case of a peptide backbone, the capping groups of neighboring fragments are placed into close proximity (see Figure 4), therefore care must be taken that the capping scheme does not overly influence the electronic coupling between fragments.

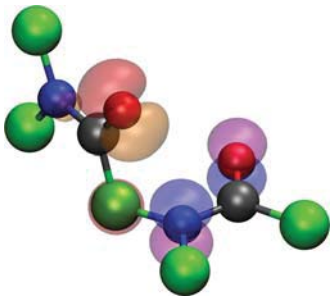

Figure 4. Two neighboring peptide fragments with overlapping connection atoms in position of the C_α atom. Pseudoatoms mimicking methyl groups are shown in green. The π_1 orbital of the N-terminal and the n_0 orbital of the C-terminal fragment is plotted. The central carbon connecting atom lies very close to the nodal plane of the π orbital, but a corresponding hydrogen link atom in its place would not.

We have selected pseudocarbon connection atoms saturating the fragments instead of the hydrogen link atoms more common in QM/MM schemes, so that the fragments are equivalent to NNDMA. Additionally, using link atoms introduces new artificial atomic centers, which could cause a significant overestimation of interfragment couplings: Figure 4 shows the connection atom placed close to the peptide bond plane, which is the expected nodal plane of the π-orbitals of a fragment. This position minimizes the influence of the connection atom to the resulting FO coupling, since even a nonzero AO expansion coefficient on the connection atom does not couple to the neighboring π_1 orbital. In comparison, a hydrogen link atom would be placed outside of this plane due to its shorter bond length, in which case the link atom orbital expansion coefficient could strongly influence the fragment coupling.

The pseudocarbon connection atom was parametrized to represent a methyl group, using the 2s basis function of carbon and one valence electron in DFTB. The alternative of representing a methyl group by a 7-electron pseudoatom with both s and p basis functions led to strong contributions of the p functions to the fragment π orbital. Carbon atom p basis functions would form sp^3 hybrid orbitals in an actual methyl group instead and would not contribute to fragment π orbitals. Therefore, a 7-electron pseudoatom, which would also lead to a higher computational cost, was rejected.

The electronic part of the DFTB2 Hamiltonian consists of the atomic orbital energies ε_μ of atomic orbitals μ on atom α, the tight binding (2-center) matrix elements $H_{\mu\nu}$ and the Hubbard parameters U_α.[65] The ss-σ and sp-σ interactions between two carbon atoms at typical single bond distances are comparable. Therefore, the interaction of the fragment with a sp^3 orbital of a capping methyl group can be very well approximated by the interaction with a 2s orbital. However, the chemical hardness of a methyl group and the energy of this bond differ substantially from the values of a 2s carbon orbital. Therefore, we decided to optimize only the pseudoatom orbital energy ε_μ and Hubbard parameter U_α in order to reproduce the IP and electron distribution of NNDMA in the capped fragments. We optimized the function

$$f(\varepsilon_\mu, U_\alpha) = \frac{|\Delta IP|}{|\Delta IP|_{MAX}} + \frac{\sqrt{\overline{\Delta q^2}}}{\sqrt{\overline{\Delta q^2}}_{MAX}} \quad (5)$$

where ΔIP is the deviation of ionization potential and $(\overline{\Delta q^2})^{1/2}$ is the root-mean-square deviation of the Mulliken atomic partial charges. This was done by plotting the function in the range of $U_\alpha \in [0.05,0.5\text{Ha/e}^2]$ and $\varepsilon_\mu \in [-0.1,-0.45\text{ eV}]$ and locating the minimum visually. Both contributions were weighted according to their respective maximum values found in the definition interval. The best fit was obtained for values of ε_i = −0.27 Ha and U_α = 0.11 Ha/e^2 (Figure 5), corresponding to ΔIP = 0.12 eV and $(\overline{\Delta q^2})^{1/2}$ = 0.038e.

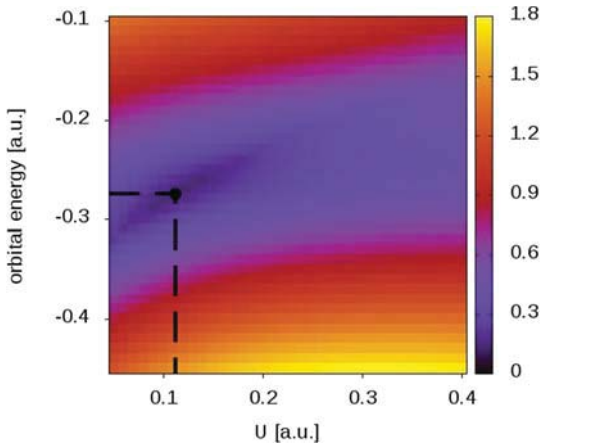

Figure 5. Parameter fit for a carbon pseudoatom imitating a methyl group. At the indicated minimum (ε_i = −0.27 Ha and U_α = 0.11 Ha/e^2), a pseudoatom-capped peptide fragment exhibits an ionization potential and charge distribution that are closest to those of NNDMA.

The optimized pseudoatom was used as capping group for all of the following fragment calculations. It was also used to cap the amino acid side chain fragments at the C_α-C_β-bond as well.

Corrections of Hamilton Matrix Elements. The energy separation between donor, acceptor and bridge levels is an important characteristic of any bridged CT system. Therefore, we compared the vacuum ΔSCF-IPs for several possible fragments obtained by DFTB and *ab initio* QM calculations. The fragments were first geometry-optimized using DFTB2, followed by a single point calculation at DFTB2, HF/TZVP, B3LYP/TZVP, PBE/TZVP and MP2/def2-TZVP level (Figure 6).[84] We find the expected order of energies, with bridge levels lying higher than donor and acceptor. All methods yield bridge energy levels ca. 1.5 eV higher than the side chain fragments, and solvent energy levels that are at least further 2.5 eV higher. This is in a good agreement with the expectations of (a) positive charges localized on the donor or acceptor side chains, (b) CT occurring through bridge-mediated tunneling instead of hopping, and (c) no relevant transport through solvent. Interestingly, the relative IP of water is strongly dependent on the QM method used, however in any case the solvent can be neglected.

In our approach a FO description is used to calculate couplings and site energies. The energetics of the CT system

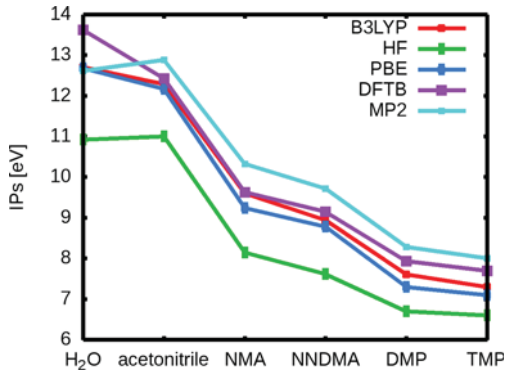

Figure 6. ΔSCF ionization potentials of donor and acceptor groups, bridge fragments and solvent, calculated in vacuum with various methods. The bridge is well separated from donor and acceptor levels. Therefore, tunneling from donor to acceptor without population of the bridge is an appropriate description. The solvent can be neglected.

are therefore described in terms of single orbital energies E_m for every fragment, instead of arguably more accurate ΔSCF-IP values; an approximation that has been shown to be valid for the case of DNA.[39] The orbital energies however show a much smaller energetic separation between donor/acceptor HOMOs and the bridge π_1 orbitals in comparison to IPs, as can be seen in Table 3. PBE and B3LYP suffer from the same underestimation of MO separation as DFTB, whereas it is overestimated using HF. To correct this shortcoming we added a constant energy offsets computed from MP2 ΔSCF-IP values to the DFTB orbital energies. The HOMO energy of 2,4-dimethoxytoluene (representing the N-terminal donor side chain) was chosen as reference point, and all of the other relevant energy levels were shifted in comparison. Note that if additionally bridge n_0 orbitals are included in the Hamiltonian, these offsets are also applied to them additionally to the shift, used to correct the orbital order for DFTB as described in a preceding section.

Special care has also to be taken of the coupling between FOs. DFTB uses a minimal basis, which is optimized to describe bonded interactions. In condensed phase atomic orbitals are compressed with respect to free orbitals in vacuum. The optimization is achieved by solving modified atomic Kohn−Sham equations to get optimized basis functions:

$$\left(-\frac{1}{2}\nabla^2 + v_{eff}(\rho_{atom}) + \left(\frac{r}{r_0}\right)^2\right)\eta_\mu = \varepsilon_\mu \eta_\mu \qquad (6)$$

where $(r/r_0)^2$ is an additional potential, only used to confine the AO basis functions. In the calculation of Hamilton matrix elements the confinement potential is omitted.

However, this procedure severely suppresses the tail of the wave function, which is crucial in order to depict the weak interaction between the individual fragments over long distances accurately. It was shown that using less confined basis funcions for the calculation of couplings between distant atoms can correct this shortcoming.[39,40] Therefore, matrix elements $H_{\mu\nu}$ in eq 2 between atoms belonging to different fragments were calculated by adapting the specially parametrized basis functions used in ref 39.

RESULTS

Peptide Dynamics from MD Simulations. To account for conformational fluctuations in the solvated model peptides, we computed electronic couplings for a set of structural snapshots taken from a 150 ns long classical MD simulation. Two sets of snapshots were taken from 10 ns long segments from the end of the full MD trajectory, one in which the peptide maintains a straight conformation and one in which it adopts a kinked structure (see Figure 7). A simulation setup

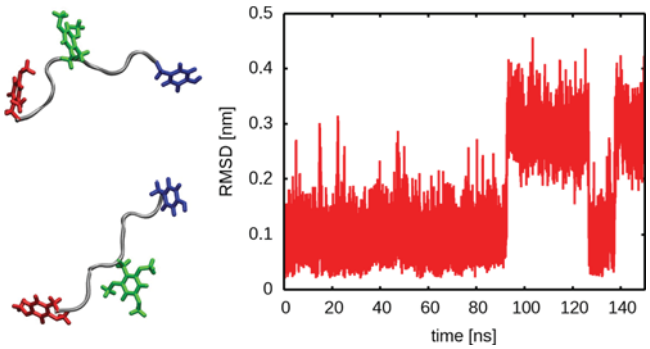

Figure 7. Two main conformations are found for the peptide over the course of 150 ns classical MD simulations. A kinked (top) and a straight (bottom) conformation can be clearly distinguished by the C_α-RMSD value (right). The structural change does not influence the DMP-TMP distance significantly.

similar to that in ref 44 was used, the difference being that the current simulations applied the same solvent mixture (water-acetonitrile) as experiments and correctly accounted for the chemical nature of the modified charge-carrying amino acid side chains. As observed before, we find a conformational equilibrium between a straight nearly ideal PPII helix and a kinked conformation, in which the helix bends around the region of the relay amino acid TMP, occupying backbone dihedral angles of ca. −15° for Ψ of the N-terminal proline before TMP and −125° for Φ of TMP, significantly different from Φ = −75° and Ψ = +150° in the regular PPII secondary structure. The straight and kinked helical structures inter-

Table 3. Comparison of HF, B3LYP, PBE and DFTB Orbital Energies to ΔSCF-IPs Computed with MP2 Perturbation Theory[a]

fragment	ΔSCF-IP^{MP2}	$E^{\pi_1}_{HF}$	$E^{\pi_1}_{B3LYP}$	$E^{\pi_1}_{PBE}$	$E^{\pi_1}_{DFTB}$	shift
2,4-dimethoxytoluene	8.28	−7.88	−5.44	−4.59	−5.55	≡0.0
2,4,6-trimethoxytoluene	8.00	−7.79	−5.26	−4.38	−5.45	0.17
NMA	10.32	−10.43	−6.72	−5.58	−6.61	−0.99
NNDMA	9.72	−9.90	−6.36	−5.26	−6.44	−0.56

[a]These serve as reference for the relative energies of fragments. HF orbital energies overestimate the height of the D-B-A barrier, whereas DFT based methods underestimate it. For DFTB, the values for pseudoatom capped fragments are shown as well as the shift used to correct the relative energies. All values are given in eV.

convert on a time scale of ca. 40 ns (too few transitions are observed to calculate an accurate rate).

IP Values of Bridge Fragments. The energetic fluctuations caused by the environment of the CT system strongly influence the energy levels of donor, acceptor and bridge fragments. Especially the solvent dynamics introduce considerable dynamical disorder. To evaluate this effect, we have averaged fragment orbital energies (including the energy shifts determined above) over 1000 equidistant conformational snapshots taken from a 10 ns long MD simulation segment and calculated standard deviations (Figure 8). Parts of the MD

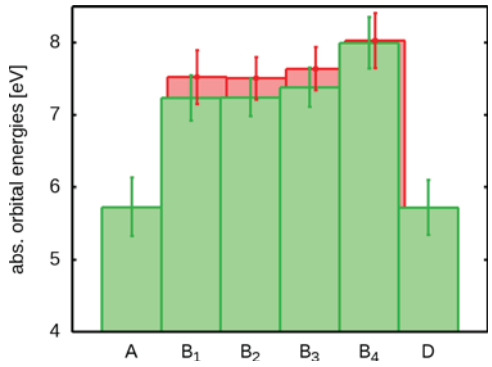

Figure 8. Absolute energy levels of the donor, acceptor and four intervening bridge fragments averaged over 10 ns long MD trajectories. HOMO levels are shown in green and HOMO-1 levels in red. Structural dynamics introduce ca. 0.3 eV of energetic fluctuations for all of the fragments. The energy separation between donor/acceptor fragments and bridge levels increases to ca. 2 eV, compared to 1.5 eV for the vacuum energies.

trajectory were chosen in which the peptide consistently occupies the straight conformation. Repeating the calculations with snapshots showing the kinked peptide geometry did not change the results significantly. We find energy fluctuations with a standard deviation of ca. 0.3 eV for all fragments. The bridge fragments appear to be stabilized by solvent interactions more strongly than the side chains, resulting in an increase in the D/A to bridge energy separation to ca. 2.0 eV, compared to 1.5 eV for the vacuum energies. For the fourth bridge fragment, closest to the central relay amino acid, the energy level is elevated slightly above the remaining bridge levels (this feature is also found in the calculations for the kinked peptide structure). The main reason for this is that the fourth fragment is equivalent to *N*-methylacetamide instead of NNDMA, with a correspondingly higher IP (Table 3).

The large energy separation between donor/acceptor energy levels and the bridge fragments at all times allows for the possibility of a bridge-mediated tunneling CT mechanism in this system. We therefore proceed to compute the donor/acceptor electronic couplings according to eq 3 in the following.

Electronic Couplings. For any given peptide structure, eq 3 can be used to compute both the direct donor–acceptor coupling V_{DA} and the bridge mediated coupling T_{DA}. Fluctuations of the energy levels, due to internal and surrounding structural changes, as well as changes in the distance and relative orientation of fragments will influence both terms. Because of the rigid nature of the PPII helix backbone, it can be expected that the comparably free rotation of the donor and acceptor amino acid side chains around their C_α–C_β and C_β–C_γ bonds is the dominating influence here.

We first turn to the direct coupling V_{DA} (Figure 9). Computing V_{DA} over the course of 10 ns MD simulation trajectories, we obtain an average value of 0.25 meV with a standard deviation of 1.27 meV for the straight peptide conformation, and an average of 0.10 meV with a standard deviation of 0.69 meV for the kinked conformation. The large standard deviations for both cases and the large fluctuations seen in Figure 9 show that molecular conformations with high CT efficiency occur only very rarely during normal thermal fluctuations. When the CT is dominated by fluctuations of the coupling, the root mean squared values should be used in rate expressions.[26] For $(\langle V_{DA}^2 \rangle)^{1/2}$, values of 1.20 and 0.69 meV are found for the straight and kinked peptide conformations, respectively.

Two main sources of error in calculating V_{DA} can be identified, first the approximations made in conducting the QM calculations and second the quality of the peptide conformational ensemble used. The first source of error has been shown to be small when comparing to DFT calculations.[39] For the second, V_{DA} values can be extremely dependent on structural changes, so even small force field inaccuracies and insufficient sampling despite long simulation times can strongly affect the results. The reported values for electronic couplings should

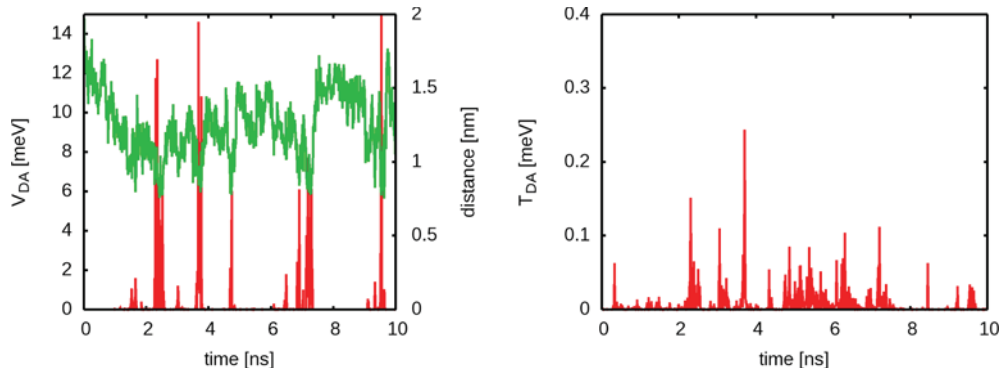

Figure 9. Time evolution of the electronic coupling between donor and acceptor over the course of a 10 ns length MD trajectory. (left) The direct coupling V_{DA} (red) is strongly distance dependent and exhibits rare spikes of up to ca. 15 meV. A short donor–acceptor center-of-mass distance (green) is necessary but not sufficient for a high coupling, since the detailed relative orientation of the π-electron systems is another crucial factor. (right) Bridge-mediated electronic couplings T_{DA} exhibit a similar pattern with a steady background coupling and less pronounced spikes however. In general, the bridge-mediated contributions T_{DA} are significantly smaller than direct couplings V_{DA}.

Table 4. Model Hamiltonian Matrix of the System[a]

		A	B_1		B_2		B_3		B_4		D
			π	n_0	π	n_0	π	n_0	π	n_0	
A		5.7276	0.0196	0.1058	0.0050	0.0091	0.0005	0.0006	0.0000	0.0001	**0.0002**
B_1	π		7.2344	0.0130	0.0456	0.2011	0.0010	0.0025	0.0000	0.0000	0.0001
	n_0			7.5237	0.0236	0.0269	0.0007	0.0023	0.0000	0.0000	0.0001
B_2	π				7.2405	0.0108	0.0463	0.2286	0.0011	0.0031	0.0016
	n_0					7.5061	0.0205	0.0354	0.0006	0.0020	0.0009
B_3	π						7.3799	0.0107	0.0423	0.2077	0.0066
	n_0							7.6394	0.0208	0.0342	0.0096
B_4	π								7.9984	0.0061	0.0589
	n_0									8.0295	0.0221
D											5.7184

[a]All values are given in eV, averaged over 10 ns length MD simulations. The data shown are for the straight peptide conformation, while very similar results are found for the kinked structure. The direct donor−acceptor coupling is highlighted in bold.

therefore be taken as semiquantitative at best. Previously, electronic couplings in such a system were reported as being significantly smaller than 1 meV.[44] The simulations reported here are longer and used a slightly different setup than those in ref 44. The difference in computed couplings can be attributed to insufficient sampling of the peptide conformational space in the previous study. High values for V_{DA} occur isolated in 2 to 3 ns intervals, with $V_{DA} \approx 0$ at all other times, a situation that makes accurate MD sampling difficult.

To compute the bridge mediated electronic couplings according to eq 3, the whole model Hamiltonian of the system is needed. Table 4 lists all average matrix elements for the straight conformation. The relative arrangement of fragments is A−B_1−B_2−B_3−B_4−D, with considerable conformational flexibility for the D and A fragments only. A common approach is to include only the highest orbital of each fragment in the Hamiltonian, which are the π_1 orbitals in the case of the bridge (for a discussion of the relative energies see previous sections). This would lead to a comparably small average T_{DA}. If however additionally the lower lying n_0 bridge orbitals are included, a significant increase in T_{DA} of about a factor of 2 from 3.0 μeV to 6.3 μeV for the straight conformation and from 0.8 μeV to 1.3 μeV for the kinked conformation is observed. The inclusion of further orbitals did not lead to a further increase of T_{DA}. At first this is surprising, since for tunneling through the n_0 orbitals the barrier is additionally 0.32 eV higher than for tunneling involving the π_1 orbitals. However, the n_0 orbitals are crucial in mediating the effective coupling between donor and acceptor. The reason for the high impact of the n_0 orbitals on T_{DA} is the high coupling between π_1 and n_0 of neighboring fragments, caused by the fortunate relative orientation in a PPII helical structure where the lone pair of the oxygen points directly at the nitrogen of the neighboring fragment as can be seen in Figure 4. Neglecting the solvent stabilization of the backbone by performing QM calculations in vacuum, T_{DA} is overestimated by a factor of about 1.5, whereas omitting the energy correction shown in Table 3 leads to a breakdown of eq 3 for several snapshots due to insufficient energetic separation of D/A and bridge levels.

The time series of T_{DA} values (Figure 9 right) has a visually similar appearance to that of V_{DA} (Figure 9 left) with rarely occurring large spikes in the computed values. However, much smaller values are found for T_{DA}, about 2 orders of magnitude below those for V_{DA}. The large fluctuations indicate that root mean squared values of T_{DA} should again be used. We find $(\langle T_{DA}^2 \rangle)^{1/2}$ of 19.4 μeV for the straight peptide conformations and 5.8 μeV for the kinked one.

Despite the existence of nonzero electronic couplings between neighboring fragments along the peptide chain, the root-mean-square bridge-mediated coupling $(\langle T_{DA}^2 \rangle)^{1/2}$ is small when compared to the direct coupling $(\langle V_{DA}^2 \rangle)^{1/2}$. Seemingly contrasting with this relation is the observation that for the most of the time in the simulations, the instantaneous T_{DA} value is larger than V_{DA}, which is evaluated as zero (exact numbers are hard to ascertain due to well-known numerical instabilities.)[17] However, since the overall coupling is heavily influenced by rare events where V_{DA} becomes much larger than T_{DA}, the former contribution to the total electronic coupling is dominant.

The calculation of the backbone mediated coupling is much more challenging than the direct donor/acceptor coupling. By using a fragment orbital approach with capping atoms possessing only s-type orbitals instead of all atom calculations, certain atomic orbitals in the boundary region which might contribute to the electronic coupling are omitted. However, as we have seen in the PPII conformation, strong couplings between neighboring fragments are possible nevertheless. Furthermore, by shifting the fragment orbital energies to match high level *ab initio* calculations, we can easily correct the energetic landscape of the charge transfer, which would be impossible in a full atomistic description.

DISCUSSION AND CONCLUSIONS

In this work, we have extended our FO framework to treat CT along the backbone of peptides and proteins:

(i) In our earlier work,[41−43] we investigated systems where the fragments have been DNA bases and peptide side chains. There, the fragmentation is easy to perform because the wave functions are naturaly localized on the respective sites. In contrast, we had to solve in this work the problem of partitioning the peptide backbone into QM fragments by representing a peptide bond with a NNDMA molecule, saturated by specially parametrized carbon-like pseudoatoms. At first sight, the fragmentation approach has the disadvantage that bonds have to be cut, which may affect the localization of the wave functions that are used to compute the electronic couplings. This problem can be ameliorated by using a special choice for the linking atoms, as investigated in detail.

(ii) Furthermore, also in contrast to earlier work we had to consider fragments with different IP values, i.e., different site energies of the FO-Hamiltonian appear which determine the energy landscape of the CT-process. A correct description of the energy landscape is critical, but as has been shown by the benchmark calculations, standard QM methods like DFT-GGA may have significant errors in the description of the HOMO energies of different molecular fragments. Even worse, also the orbital ordering along the backbone is described pretty differently using different methods. This is related to the approximate character of the exchange-correlation functionals. A similar error, however, can in principle also occur in other semiempirical and tight-binding approaches. Therefore, an all-atom description of the entire system can in principle lead to erroneous results, since the energetics of the functional groups along the CT pathway may not be correct. With a fragment approach this error can be taken care of. Therefore, our fragmentation scheme is optimized with respect to the IP values of the fragment molecules and uses high level *ab initio* QM calculations to obtain a correct ordering of fragment orbital energies as well as relative energies of donor bridge and acceptor.

(iii) Further, we have extended the FO Hamiltonian to include two orbitals per site, which in principle can easily be extended to an arbitrary number of orbitals per site. In a first step, we only used the π-orbitals along the backbone. Including also the σ-orbitals, we found an increase in the couplings by a factor of 2. Although the barrier for tunneling through these orbitals is higher than for the π-orbitals, they lead to additional bridge states which enhance the tunneling by providing alternative pathways when the coupling between π-orbitals is small.

This strategy leads to a very efficient approach, since only small, nonoverlapping fragments have to be computed, which leads to a linear scaling of computing time with system size. We further apply DFTB as quantum method in the FO approach leads to a computational speedup of about 3 orders of magnitude compared to standard DFT approaches with medium sized basis sets. As shown recently, DFTB computes couplings with similar accuracy as full DFT within the FO approach.[39,85] However, since DFTB also suffers from the well-known DFT problems described above, the correction of site energies is a mandatory procedure. Therefore, applying the FO approach seems to be a virtue instead of an additional approximation, since it allows to compute a correct CT energy landscape. As has pointed out earlier, the use of semiempirical methods in an AO basis may not lead to reliable results.[38] This finding may be related to the description of the correct CT energy landscape.

In contrast to many earlier work, our FO approach includes the coupling to the environment via QM/MM. In this way, the site energy of the FO is directly influenced by the rest of the system, in particular by polar solvents. As detailed in our earlier work, the fluctuations of the site energies in the order of 0.3 eV mostly result from fluctuations in the polar environment,[40] the fluctuations of the geometry of the individual sites are much smaller. These solvent fluctuations can be considered to be a major driving force for CT.

In addition, however, we find a large solvent-induced shift of the bridge states wrt to the D/A states, thereby increasing the barrier due to solvent effects. This effect would be completely missing when omitting the QM/MM coupling. We therefore suggest that solvated peptides are not a particularly good models for CT in proteins. In proteins, CT efficiency can be expected to be larger than in this solvated peptide because the protein interior is less polar than aqueous solution, which leads to a smaller D/A to bridge energy separation, favoring CT through the backbone.

Further, in proteins donor and acceptor molecules are typically embedded in a stable protein tertiary/quaternary structure, which can provide efficient static CT pathways. We calculated the electronic couplings for a series of MD snapshots of the peptide system for direct and bridge-mediated donor−acceptor interactions separately and find that in average the direct coupling between donor and acceptor side chains is dominant and that it is strongly influenced by the flexibility of the side chains. We obtain comparably small couplings in the meV range or below in all cases, as expected for CT between moieties at intermediate molecular distance, i.e., beyond van der Waals contact. The relatively free mutual movement of the donor and acceptor side chains results in very large fluctuations of V_{DA}, where D/A orientations which are favorable for CT are very rare, but show significant couplings. As shown above, these conformations occur roughly once every nanosecond with couplings in the order of 5−10 meV. This may allow for direct hopping transfer, although with low efficiency, which may not be well described by averages of the couplings.

Recently, we have computed the couplings for the same system using an empirical pathway model,[44] finding comparable average couplings around 0,2 meV. Despite the similar outcome, one difference between the methods should be mentioned: The empirical pathway model is parametrized for some reference systems and has been mainly applied to CT within proteins, where a much smaller dielectric constant is present. Therefore, we can expect that the increase of the barrier due to the fact, that the CT pathway in the peptide is exposed to the solvent is not included in the pathway model.

However, neither of the theoretical approaches are able to quantitatively reproduce experimental rates, they are underestimated by several orders of magnitude as discussed in detail in ref 44. This can have several reasons: First, the calculated λ values[44] are in the order of 2 eV, which is very large compared to values found for proteins,[86] and determine the slow computed rates. It is likely that the computational approaches to estimate λ tend to overestimate its value. Second, the presupposed charge transfer mechanism may not be operative in this system. There are at least two alternatives: On the one hand, our simulations indicate that due to the structural flexibility a direct D−A occurs in the ns time regime. This rate is very sensitive to the force field accuracy: since the couplings are very sensitive to the structures, a slightly wrong representation of the free energy surface by the force fields can lead to large errors. Therefore, there is the possibility that the a direct D−A contact is mainly responsible for the CT in this system. Further, there are many conformations where D and A are separated by one or only few water molecules. A significant amount of CT could also occur via such water bridges, which are very difficult to include in the calculations. In this case, the couplings can not simply be averaged, and the above equation is not applicable. Further, there one can not exclude a contribution from thermally induced hopping via bridge population. Experiments investigating the distance dependence of CT report a change in transfer mechanism for

3−4 proline spacer.[87] For smaller peptides, superexchange tunneling is prevalent, while for longer poly proline helices thermally induced hopping via bridge states tends to dominate. The peptide investigated here has a length which is at the transition region, therefore, backbone population may contribute to the total charge transfer and the pure tunneling description may not be appropriate any more. On the other hand, the energy separation from donor to the bridge is quite large, mainly due to the presence of the solvent, that this pathway seems to be less likely.

Although these small solvated peptides seemed to be simple systems which would allow to study CT in a well controlled way, they turned out to be rather complicated objects, emphasizing the need to develop CT methods, which allow to describe the transition between tunneling and hopping in a more flexible way.

AUTHOR INFORMATION

Corresponding Authors

*(M.E.) E-mail: marcus.elstner@kit.edu. Telephone: +49 (0) 721 608 45705. Fax: +49 (0)721 608 45710.

*(T.B.S.) E-mail: thomas.steinbrecher@kit.edu.

Notes

The authors declare no competing financial interest.

ACKNOWLEDGMENTS

T.B.S. is indebted to the Baden-Württemberg Stiftung for the financial support of this research project by the Eliteprogramme for Postdocs. S.S. thanks the University of Cyprus for providing financial support for the visit of P.B.W.

REFERENCES

(1) Warshel, A. Molecular Dynamics Simulations of Biological Reactions. *Acc. Chem. Res.* **2002**, *35*, 385−395.

(2) Schultz, B. E.; Chan, S. I. Structures and Proton-Pumping Strategies of Mitochondiral Respiratory Enzymes. *Annu. Rev. Biophys. Biomol. Struct.* **2001**, *30*, 23−65.

(3) Marcus, R. A. Electron Transfer Reactions in Chemistry. Theory and Experiment. *Rev. Mod. Phys.* **1993**, *65*, 599−610.

(4) Marcus, R. A. Electron Transfer Past and Future. *Adv. Chem. Phys.* **1999**, *106*, 1−6.

(5) Hervás, M.; Navarro, J. A.; De la Rosa, M. A. Electron Transfer between Membrane Complexes and Soluble Proteins in Photosynthesis. *Acc. Chem. Res.* **2003**, *36*, 798−805.

(6) Bixon, M.; Jortner, J. Electron Transfer-from Isolated Molecules to Biomolecules. *Adv. Chem. Phys.* **1999**, *106*, 35−202.

(7) Gray, H. B.; Winkler, J. R. Electron Transfer in Proteins. *Annu. Rev. Biochem.* **1996**, *65*, 537−561.

(8) Marcus, R. A. On the Theory of Oxidation-Reduction Reactions Involving Electron Transfer. I. *J. Chem. Phys.* **1956**, *24*, 966−978.

(9) Marcus, R. A. Electrostatic Free Energy and Other Properties of States Having Nonequilibrium Polarization. I. *J. Chem. Phys.* **1956**, *24*, 979−989.

(10) Marcus, R. A. Chemical and Electrochemical Electron-Transfer Theory. *Annu. Rev. Phys. Chem.* **1964**, *15*, 155−196.

(11) Marcus, R.; Sutin, N. Electron Transfers in Chemistry and Biology. *Biochim. Biophys. Acta* **1985**, *811*, 265−322.

(12) Levich, V. G.; Dogonadze, R. R. Theory of Non-Radiation Electron Transitions from Ion to Ion in Solutions. *Dokl. Akad. Nauk SSSR* **1959**, *124*, 123−126.

(13) Hush, N. S. Adiabatic Theory of Outer Sphere Electron-Transfer Reactions in Solution. *Trans. Faraday Soc.* **1961**, *57*, 557−580.

(14) Hopfield, J. J. Electron Transfer between Biological Molecules by Thermally Activated Tunneling. *Proc. Natl. Acad. Sci. U.S.A.* **1974**, *71*, 3640−3644.

(15) Jortner, J. Temperature Dependent Activation Energy for Electron Transfer between Biological Molecules. *J. Chem. Phys.* **1976**, *64*, 4860−4867.

(16) Moser, C. C.; Keske, J. M.; Warncke, K.; Farid, R. S.; Dutton, P. L. Nature of Biological Electron Transfer. *Nature* **1992**, *355*, 796−802.

(17) de la Lande, A.; Salahub, D. R. Derivation of Interpretative Models for Long Range Electron Transfer from Constrained Density Functional Theory. *J. Mol. Struct. (THEOCHEM)* **2010**, *943*, 115−120.

(18) de la Lande, A.; Babcock, N. S.; Řezáč, J.; Sanders, B. C.; Salahub, D. R. Surface Residues Dynamically Organize Water Bridges to Enhance Electron Transfer between Proteins. *Proc. Natl. Acad. Sci. U.S.A.* **2010**, *107*, 11799−11804.

(19) Hammi, E. E.; Houee-Levin, C.; Rezac, J.; Levy, B.; Demachy, I.; Baciou, L.; de la Lande, A. New Insights into the Mechanism of Electron Transfer within Flavohemoglobins: Tunnelling Pathways, Packing Density, Thermodynamic and Kinetic Analyses. *Phys. Chem. Chem. Phys.* **2012**, *14*, 13872−13880.

(20) Medvedev, D. M.; Daizadeh, I.; Stuchebrukhov, A. A. Electron Transfer Tunneling Pathways in Bovine Heart Cytochrome c Oxidase. *J. Am. Chem. Soc.* **2000**, *122*, 6571−6582.

(21) Tan, M.-L.; Balabin, I.; Onuchic, J. N. Dynamics of Electron Transfer Pathways in Cytochrome c Oxidase. *Biophys. J.* **2004**, *86*, 1813−1819.

(22) Prytkova, T. R.; Kurnikov, I. V.; Beratan, D. N. Ab Initio Based Calculations of Electron-Transfer Rates in Metalloproteins. *J. Phys. Chem. B* **2005**, *109*, 1618−1625.

(23) Kim, J.; Stuchebrukhov, A. Ab Initio Study of Long-Distance Electron Tunneling in a Model Peptide System. *J. Phys. Chem. B* **2000**, *104*, 8606−8613.

(24) Oberhofer, H.; Blumberger, J. Insight into the Mechanism of the Ru2+-Ru3+ Electron Self-Exchange Reaction from Quantitative Rate Calculations. *Angew. Chem., Int. Ed.* **2010**, *49*, 3631−3634.

(25) Wallrapp, F. H.; Voityuk, A. A.; Guallar, V. In-silico Assessment of Protein-Protein Electron Transfer. A Case Study: Cytochrome c Peroxidase - Cytochrome c. *PLoS Comput. Biol.* **2013**, *9*, e1002990.

(26) Skourtis, S. S.; Waldeck, D. H.; Beratan, D. N. Fluctuations in Biological and Bioinspired Electron-Transfer Reactions. *Annu. Rev. Phys. Chem.* **2010**, *61*, 461−485.

(27) Beratan, D. N.; Skourtis, S. S.; Balabin, I. A.; Balaeff, A.; Keinan, S.; Venkatramani, R.; Xiao, D. Steering Electrons on Moving Pathways. *Acc. Chem. Res.* **2009**, *42*, 1669−1678.

(28) Balabin, I. A.; Beratan, D. N.; Skourtis, S. S. Persistence of Structure over Fluctuations in Biological Electron-Transfer Reactions. *Phys. Rev. Lett.* **2008**, *101*, 158102.

(29) Grozema, F. C.; Siebbeles, L. D. A.; Berlin, Y. A.; Ratner, M. A. Hole Mobility in DNA: Effects of Static and Dynamic Structural Fluctuations. *ChemPhysChem* **2002**, *3*, 536−539.

(30) Grozema, F. C.; Berlin, Y. A.; Siebbeles, L. D. A. Mechanism of Charge Migration through DNA: Molecular Wire Behavior, Single-Step Tunneling or Hopping? *J. Am. Chem. Soc.* **2000**, *122*, 10903−10909.

(31) Hatcher, E.; Balaeff, A.; Keinan, S.; Venkatramani, R.; Beratan, D. N. PNA versus DNA: Effects of Structural Fluctuations on Electronic Structure and Hole-Transport Mechanisms. *J. Am. Chem. Soc.* **2008**, *130*, 11752−11761.

(32) Zhang, J.; Albrecht, T.; Chi, Q.; Kuznetsov, A. M.; Ulstrup, J. Chapter Charge Transfer and Interfacial Bioelectrochemistry at the Nanoscale and Single-Molecule Levels. In *Bioinorganic Electrochemistry*; Ulstrup, J., Hammerich, O., Eds.; Springer: Dordrecht, The Netherlands, 2008; pp 249−302.

(33) Cortés, E.; Etchegoin, P. G.; Le Ru, E. C.; Fainstein, A.; Vela, M. E.; Salvarezza, R. C. Strong Correlation between Molecular Configurations and Charge-Transfer Processes Probed at the Single-Molecule Level by Surface-Enhanced Raman Scattering. *J. Am. Chem. Soc.* **2013**, *135*, 2809−2815.

(34) Kawai, K.; Matsutani, E.; Maruyama, A.; Majima, T. Probing the Charge-Transfer Dynamics in DNA at the Single-Molecule Level. *J. Am. Chem. Soc.* **2011**, *133*, 15568−15577.
(35) Newton, M. D.; Boer, F. P.; Lipscomb, W. N. Molecular Orbital Theory for Large Molecules. Approximation of the SCF LCAO Hamiltonian Matrix1. *J. Am. Chem. Soc.* **1966**, *88*, 2353−2360.
(36) Closs, G. L.; Miller, J. R. Intramolecular Long-Distance Electron Transfer in Organic Molecules. *Science* **1988**, *240*, 440−447.
(37) Shephard, M. J.; Paddon-Row, M. N.; Jordan, K. D. Electronic Coupling through Saturated Hydrocarbon Bridges. *Chem. Phys.* **1993**, *176*, 289−304.
(38) Kurnikov, I. V.; Beratan, D. N. Ab initio Based Effective Hamiltonians for Long-Range Electron Transfer: Hartree-Fock Analysis. *J. Chem. Phys.* **1996**, *105*, 9561−9573.
(39) Kubař, T.; Woiczikowski, P. B.; Cuniberti, G.; Elstner, M. Efficient Calculation of Charge-Transfer Matrix Elements for Hole Transfer in DNA. *J. Phys. Chem. B* **2008**, *112*, 7937−7947.
(40) Kubař, T.; Elstner, M. What Governs the Charge Transfer in DNA? The Role of DNA Conformation and Environment. *J. Phys. Chem. B* **2008**, *112*, 8788−8798.
(41) Kubař, T.; Gutiérrez, R.; Kleinekathöfer, U.; Cuniberti, G.; Elstner, M. Modeling Charge Transport in DNA Using Multi-Scale Methods. *Phys. Status Solidi B* **2013**, *250*, 2277−2287.
(42) Kubař, T.; Elstner, M. Efficient Algorithms for the Simulation of Non-Adiabatic Electron Transfer in Complex Molecular Systems: Application to DNA. *Phys. Chem. Chem. Phys.* **2013**, *15*, 5794−5813.
(43) Kubař, T.; Elstner, M. A Hybrid Approach to Simulation of Electron Transfer in Complex Molecular Systems. *J. R. Soc. Interface* **2013**, *10*, 20130415.
(44) Heck, A.; Woiczikowski, P. B.; Kubař, T.; Giese, B.; Elstner, M.; Steinbrecher, T. B. Charge Transfer in Model Peptides: Obtaining Marcus Parameters from Molecular Simulation. *J. Phys. Chem. B* **2012**, *116*, 2284−2293.
(45) Cordes, M.; Jacques, O.; Köttgen, A.; Jasper, C.; Boudebous, H.; Giese, B. Development of a Model System for the Study of Long Distance Electron Transfer in Peptides. *Adv. Synth. Catal.* **2008**, *350*, 1053−1062.
(46) Giese, B.; Napp, M.; Jacques, O.; Boudebous, H.; Taylor, A. M.; Wirz, J. Multistep Electron Transfer in Oligopeptides: Direct Observation of Radical Cation Intermediates. *Angew. Chem., Int. Ed.* **2005**, *44*, 4073−4075.
(47) Meggers, E.; Michel-Beyerle, M. E.; Giese, B. Sequence Dependent Long Range Hole Transport in DNA. *J. Am. Chem. Soc.* **1998**, *120*, 12950−12955.
(48) Meggers, E.; Kusch, D.; Spichty, M.; Wille, U.; Giese, B. Electron Transfer through DNA in the Course of Radical-Induced Strand Cleavage. *Angew. Chem., Int. Ed.* **1998**, *37*, 460−462.
(49) Cordes, M.; Giese, B. Electron Transfer in Peptides and Proteins. *Chem. Soc. Rev.* **2009**, *38*, 892−901.
(50) Giese, B.; Wang, M.; Gao, J.; Stoltz, M.; Müller, P.; Graber, M. Electron Relay Race in Peptides. *J. Org. Chem.* **2009**, *74*, 3621−3625.
(51) Wang, M.; Gao, J.; Müller, P.; Giese, B. Electron Transfer in Peptides with Cysteine and Methionine as Relay Amino Acids. *Angew. Chem., Int. Ed.* **2009**, *48*, 4232−4234.
(52) Gao, J.; Müller, P.; Wang, M.; Eckhardt, S.; Lauz, M.; Fromm, K. M.; Giese, B. Electron Transfer in Peptides: The Influence of Charged Amino Acids. *Angew. Chem., Int. Ed.* **2011**, *50*, 1926−1930.
(53) Priyadarshy, S.; Skourtis, S. S.; Risser, S. M.; Beratan, D. N. Bridge-Mediated Electronic Interactions: Differences between Hamiltonian and Green Function Partitioning in a Non-Orthogonal Basis. *J. Chem. Phys.* **1996**, *104*, 9473−9481.
(54) Skourtis, S. S.; Archontis, G.; Xie, Q. Electron Transfer through Fluctuating Bridges: On the Validity of the Superexchange Mechanism and Time-Dependent Tunneling Matrix Elements. *J. Chem. Phys.* **2001**, *115*, 9444−9462.
(55) Xie, Q.; Archontis, G.; Skourtis, S. S. Protein Electron Transfer: a Numerical Study of Tunneling through Fluctuating Bridges. *Chem. Phys. Lett.* **1999**, *312*, 237−246.
(56) Hornak, V.; Abel, R.; Okur, A.; Strockbine, B.; Roitberg, A.; Simmerling, C. Comparison of Multiple Amber Force Fields and Development of Improved Protein Backbone Parameters. *Proteins* **2006**, *65*, 712−725.
(57) Bayly, C. I.; Cieplak, P.; Cornell, W.; Kollman, P. A. A Well-behaved Electrostatic Potential Based Method Using Charge Restraints for Deriving Atomic Charges: the RESP Model. *J. Phys. Chem.* **1993**, *97*, 10269−10280.
(58) Horn, H. W.; Swope, W. C.; Pitera, J. W.; Madura, J. D.; Dick, T. J.; Hura, G. L.; Head-Gordon, T. Development of an Improved Four-site Water Model for Biomolecular Simulations: TIP4P-Ew. *J. Chem. Phys.* **2004**, *120*, 9665−9678.
(59) Horn, H. W.; Swope, W. C.; Pitera, J. W. Characterization of the TIP4P-Ew Water Model: Vapor Pressure and Boiling Point. *J. Chem. Phys.* **2005**, *123*, 194504.
(60) Guàrdia, E.; Pinzón, R.; Casulleras, J.; Orozco, M.; Luque, F. J. Comparison of Different Three-site Interaction Potentials for Liquid Acetonitrile. *Mol. Simul.* **2001**, *26*, 287−306.
(61) Van Der Spoel, D.; Lindahl, E.; Hess, B.; Groenhof, G.; Mark, A. E.; Berendsen, H. J. C. GROMACS: Fast, Flexible, and Free. *J. Comput. Chem.* **2005**, *26*, 1701−1718.
(62) Hess, B.; Kutzner, C.; van der Spoel, D.; Lindahl, E. GROMACS 4: Algorithms for Highly Efficient, Load-Balanced, and Scalable Molecular Simulation. *J. Chem. Theory Comput.* **2008**, *4*, 435−447.
(63) Hess, B. P-LINCS: A Parallel Linear Constraint Solver for Molecular Simulation. *J. Chem. Theory Comput.* **2007**, *4*, 116−122.
(64) Porezag, D.; Frauenheim, T.; Köhler, T.; Seifert, G.; Kaschner, R. Construction of Tight-Binding-like Potentials on the Basis of Density-Functional Theory: Application to Carbon. *Phys. Rev. B* **1995**, *51*, 12947−12957.
(65) Elstner, M.; Porezag, D.; Jungnickel, G.; Elsner, J.; Haugk, M.; Frauenheim, T.; Suhai, S.; Seifert, G. Self-Consistent-Charge Density-Functional Tight-Binding Method for Simulations of Complex Materials Properties. *Phys. Rev. B* **1998**, *58*, 7260−7268.
(66) Troisi, A.; Orlandi, G. The Hole Transfer in DNA: Calculation of Electron Coupling between Close Bases. *Chem. Phys. Lett.* **2001**, *344*, 509−518.
(67) Senthilkumar, K.; Grozema, F. C.; Guerra, C. F.; Bickelhaupt, F. M.; Lewis, F. D.; Berlin, Y. A.; Ratner, M. A.; Siebbeles, L. D. A. Absolute Rates of Hole Transfer in DNA. *J. Am. Chem. Soc.* **2005**, *127*, 14894−14903.
(68) Löwdin, P. O. On the Non-Orthogonality Problem Connected with the Use of Atomic Wave Functions in the Theory of Molecules and Crystals. *J. Chem. Phys.* **1950**, *18*, 365−375.
(69) Sweigart, D. A.; Turner, D. W. Lone Pair Orbitals and their Interactions Studied by Photoelectron Spectroscopy. I. Carboxylic Acids and their Derivatives. *J. Am. Chem. Soc.* **1972**, *94*, 5592−5598.
(70) Humphrey, W.; Dalke, A.; Schulten, K. VMD: Visual Molecular Dynamics. *J. Mol. Graph.* **1996**, *14*, 33−38.
(71) Baranov, L. Y.; Schlag, E. W. New Mechanism for Facile Charge Transport in Polypeptides. *Z. Naturforsch.* **1999**, *54*, 387−396.
(72) Møller, C.; Plesset, M. S. Note on an Approximation Treatment for Many-Electron Systems. *Phys. Rev.* **1934**, *46*, 618−622.
(73) Head-Gordon, M.; Pople, J. A.; Frisch, M. J. MP2 Energy Evaluation by Direct Methods. *Chem. Phys. Lett.* **1988**, *153*, 503−506.
(74) Löwdin, P. O. Quantum Theory of Many-Particle Systems. I. Physical Interpretations by Means of Density Matrices, Natural Spin-Orbitals, and Convergence Problems in the Method of Configurational Interaction. *Phys. Rev.* **1955**, *97*, 1474−1489.
(75) Roos, B. O.; Taylor, P. R.; Siegbahn, P. E. M. A Complete Active Space SCF Method (CASSCF) Using a Density Matrix Formulated Super-CI Approach. *Chem. Phys.* **1980**, *48*, 157−173.
(76) Neese, F. The ORCA Program System. *WIREs Comput. Mol. Sci.* **2012**, *2*, 73−78.
(77) Hedin, L. New Method for Calculating the One-Particle Green's Function with Application to the Electron-Gas Problem. *Phys. Rev.* **1965**, *139*, A796−A823.
(78) Rinke, P.; Qteish, A.; Neugebauer, J.; Freysoldt, C.; Scheffler, M. Combining GW Calculations with Exact-Exchange Density-Functional

Theory: An Analysis of Valence-Band Photoemission for Compound Semiconductors. *New J. Phys.* **2005**, *7*, 126.
(79) Niehaus, T. A.; Rohlfing, M.; Della Sala, F.; Di Carlo, A.; Frauenheim, T. Quasiparticle Energies for Large Molecules: A Tight-Binding-Based Green's-Function Approach. *Phys. Rev. A* **2005**, *71*, 022508.
(80) Antes, I.; Thiel, W. Adjusted Connection Atoms for Combined Quantum Mechanical and Molecular Mechanical Methods. *J. Phys. Chem. A* **1999**, *103*, 9290−9295.
(81) Zhang, Y.; Lee, T. S.; Yang, W. A Pseudobond Approach to Combining Quantum Mechanical and Molecular Mechanical Methods. *J. Chem. Phys.* **1999**, *110*, 46−54.
(82) Hu, H.; Yang, W. Development and Application of ab initio QM/MM Methods for Mechanistic Simulation of Reactions in Solution and in Enzymes. *J. Mol. Struct. (THEOCHEM)* **2009**, *898*, 17−30.
(83) Senn, H. M.; Thiel, W. QM/MM Methods for Biomolecular Systems. *Angew. Chem., Int. Ed.* **2009**, *48*, 1198−1229.
(84) Weigend, F.; Ahlrichs, R. Balanced Basis Sets of Split Valence, Triple Zeta Valence and Quadruple Zeta Valence Quality for H to Rn: Design and Assessment of Accuracy. *Phys. Chem. Chem. Phys.* **2005**, *7*, 3297−3305.
(85) Kubas, A.; Hoffmann, F.; Heck, A.; Oberhofer, H.; Elstner, M.; Blumberger, J. Electronic Couplings for Molecular Charge Transfer: Benchmarking CDFT, FODFT and FODFTB against High-Level ab initio Calculations. *J. Chem. Phys.* **2014**, *140*, 104105.
(86) Moser, C. C.; Anderson, R. L.; Dutton, P. L. Guidelines for Tunneling in Enzymes. *Biochim. Biophys. Acta* **2010**, *1797*, 1573−1586.
(87) Malak, R. A.; Gao, Z.; Wishart, J. F.; Isied, S. S. Long-Range Electron Transfer Across Peptide Bridges: The Transition from Electron Superexchange to Hopping. *J. Am. Chem. Soc.* **2004**, *126*, 13888−13889.
(88) The planewave code *PWSCF* was applied for DFT calculations using the LDA functional with a cutoff of 65 Ry for the wave function (260 Ry for the density). The simulation box was 35 × 35 × 35 bohr. The subsequent GW-calculation was performed with a (box-)cutoff for the coulomb interactions. 3000 bands were taken into account. After a first G_0W_0 calculation the obtained HOMO−LUMO gap was used as scissor correction in the calculation of the polarizability and dielectric constant.